



HAL
open science

Effects of cementite size and chemistry on the kinetics of austenite formation during heating of a high-formability steel

Arthur Marceaux Dit Clément, Khalid Hoummada, Josée Drillet, Véronique Hébert, Philippe Maugis

► To cite this version:

Arthur Marceaux Dit Clément, Khalid Hoummada, Josée Drillet, Véronique Hébert, Philippe Maugis. Effects of cementite size and chemistry on the kinetics of austenite formation during heating of a high-formability steel. *Computational Materials Science*, 2020, 182, pp.109786. 10.1016/j.commatsci.2020.109786 . hal-02570419

HAL Id: hal-02570419

<https://hal.science/hal-02570419v1>

Submitted on 22 Aug 2022

HAL is a multi-disciplinary open access archive for the deposit and dissemination of scientific research documents, whether they are published or not. The documents may come from teaching and research institutions in France or abroad, or from public or private research centers.

L'archive ouverte pluridisciplinaire **HAL**, est destinée au dépôt et à la diffusion de documents scientifiques de niveau recherche, publiés ou non, émanant des établissements d'enseignement et de recherche français ou étrangers, des laboratoires publics ou privés.



Distributed under a Creative Commons Attribution - NonCommercial 4.0 International License

Effects of cementite size and chemistry on the kinetics of austenite formation during heating of a high-formability steel

Arthur Marceaux dit Clément^{a,b,*}, Khalid Hoummada^a, Josée Drillet^b, Véronique Hébert^b,
Philippe Maugis^a

^aAix Marseille Univ, CNRS, IM2NP, Campus de Saint Jérôme - Case 142, Avenue Escadrille
Normandie Niemen, F-13397 MARSEILLE Cedex 20, France

^bArcelorMittal Maizières Research SA, Voie Romaine, 57280 Maizières les Metz, France

* Corresponding author: Arthur Marceaux dit Clément
arthur.marceauxditclement@arcelormittal.com
ArcelorMittal Research SA
Voie Romaine
57280 Maizières-lès-Metz
FRANCE

Authors e-mail addresses

- Khalid Hoummada: khalid.hoummada@im2np.fr
- Josée Drillet: josee.drillet@arcelormittal.com
- Véronique Hébert: veronique.hebert@arcelormittal.com
- Philippe Maugis: philippe.maugis@im2np.fr

Abstract

To understand how austenite forms in high-formability steels during the heating step of intercritical annealing, calculations based on atomic diffusion and local equilibrium assumption were used to simulate the transformation kinetics. It appears that chromium must be considered in the calculations to allow for a good fit with the austenite formation kinetics obtained by dilatometry. Indeed, Cr has a strong delaying effect on this kinetics, even though it is a minor element in the steel chemistry. The parametric study reveals that cementite initial radius is the most influential parameter on transformation kinetics. Mn and Cr enrichments also prove to be important parameters to consider.

Keywords

Cementite; austenite; simulation; intercritical annealing; steel

Highlights

- Cr has to be considered to correctly simulate non-isothermal austenitization kinetics
- Cr affects austenitization kinetics by modifying Mn fluxes at α/γ interface
- Cementite radius is the most influential parameter on austenitization kinetics

1. Introduction

High-strength steels are widely used in the automotive industry to help reduce the average weight of vehicles without compromising passenger safety [1–3]. Manufacturing of these steels involves several complex steps at high temperature (continuous casting, hot rolling, coiling) and at ambient temperature (cold rolling). This last step precedes intercritical annealing, during which a certain amount of austenite (γ) is formed. The way austenite decomposes upon cooling gives the steel its final microstructure and therefore its mechanical properties.

During intercritical heating of a cold-rolled bainite-martensite initial microstructure, recrystallization and cementite (θ) precipitation occur simultaneously [4,5]. As austenite forms from a mixture of ferrite (α) and cementite following the eutectoid reaction $\alpha + \theta \rightarrow \gamma$, it is of prime importance to determine how a variation of cementite size or chemistry can affect austenite formation kinetics during intercritical heating. These parameters are indeed variable from one steel to another, as they depend on all previous manufacturing steps. It is therefore difficult to accurately predict cementite size or chemistry at the beginning of austenite formation during intercritical heating.

Austenite formation has been extensively studied for a variety of initial microstructures under isothermal conditions [6–16]. It has been shown that, still under isothermal conditions, increasing nominal Mn content delays austenite formation kinetics (AFK) [8,17]. There is however a lack of studies on the influence of cementite initial Mn enrichment on AFK [12,18]. It can be assumed that varying the initial cementite composition will lead to a change in AFK, as changing cementite Mn or Cr content will affect the set of operative tie-lines of austenitic transformation [12]. Similarly, under isothermal conditions, increasing nominal Cr content leads to delayed austenitization [8,11,17] but the influence of cementite initial Cr enrichment on AFK has not been studied either. The same conclusion can be drawn for different particle sizes [8], even though it is commonly accepted that larger particles lead to slower austenitization kinetics. Moreover, very few studies take interest in studying the importance of these parameters under *anisothermal* conditions. As diffusivities and equilibrium conditions evolve with temperature, transformation kinetics will vary from isothermal cases. The existing works usually consider very high heating rates, very simple chemical compositions or put aside the redistribution of substitutional elements between ferrite and austenite [16,19–21]. **Studies led on conventional heating rates [19,20,22] or quaternary systems [23,24] are scarce.** Available literature thus lacks studies about anisothermal austenitization and the influence of cementite chemistry on austenitization kinetics.

In this work, 1°C/s heating of a high-formability steel is considered. Growth of austenite is studied by calculations assuming sharp interfaces and local equilibrium holding on them. To this end, Thermo-Calc and DICTRA softwares [25] were used. Fluxes evolution on the transformation interface will be used to show how Cr affects the transformation kinetics. Indeed, the combination of evolving diffusivities, compositions and activities with temperature makes this approach more adapted to the analysis of non-isothermal transformation kinetics than composition/activities gradients only. The effects of cementite size and Mn or Cr enrichment on austenite formation kinetics were also investigated.

2. Materials and methods

Table 1 – Nominal chemical composition of studied steel.

	C	Mn	Cr	Si	Other elements
[wt.%]	0.197	2.57	0.306	0.916	Al, Nb, Ti, B
[at.%]	0.9	2.57	0.323	1.79	

The steel grade investigated in this work was elaborated in ArcelorMittal Research Center in Maizières-lès-Metz, France. Its nominal chemical composition is given in **Table 1**. The initial microstructure after hot rolling and coiling at 545°C was made of 60% bainite and 40% martensite. Cold rolling (50% reduction) was then applied. Slow heating (1°C/s heating rate) was performed in a DT1000 dilatometer, and interruption at desired temperatures done by helium blowing. SEM micrographs were obtained on a FEG-SEM JEOL® JSM-7800F at quarter steel sheet thickness. Cementite, austenite and ferrite grain boundaries were revealed by Dino etching (140 mL distilled water, 100 mL H₂O₂, 4 g oxalic acid, 2 mL H₂SO₄, 1.5 mL HF) after conventional metallographic polishing. **To determine the mean chemistry of cementite before austenite formation, cementite particles were first extracted from the ferritic matrix by electrolytic extraction. The dimensions of the steel sample were of approximately 10 squared centimeters with 1.25 mm thickness. Mass of the sample was of about 10 grams. Extraction residues were then analyzed by inductively-coupled plasma mass spectrometry (ICP-MS).**

Calculations are conducted using Thermo-Calc 2018b and DICTRA softwares with TCFE9 thermodynamical database [26] and MOB2 mobility database [27]. The absence of mobility data for Si in cementite in MOB2 database prevents the consideration of this element in the calculations. DICTRA default parameters are kept unchanged for austenite nucleation, which starts when the driving force for nucleation exceeds $\Delta G = 10^{-5}RT$.

3. Results

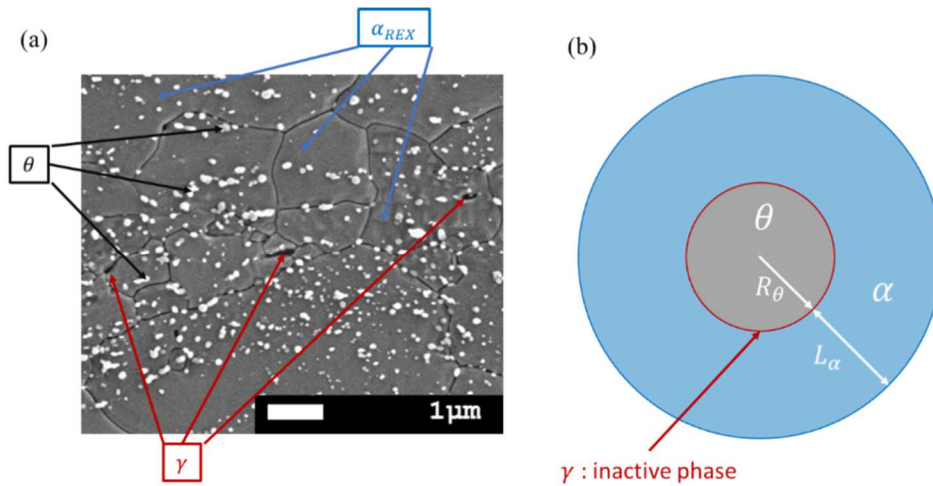


Figure 1 – (a) SEM micrograph (DINO etching) of the studied steel after 1°C/s heating up to 710°C (Ac1 temperature). Cementite carbides are relatively homogeneously dispersed in the almost 100%-recrystallized ferritic matrix. – (b) 2D representation of the chosen spherical DICTRA geometry to simulate austenite growth. The cementite particle is embedded in a ferrite shell.

Figure 1 (a) shows the microstructure of the steel after 1°C/s heating up to 710°C, temperature at which austenite starts to form (Ac1 = 710°C). Recrystallization is almost complete. Cementite particles (in white) are homogeneously dispersed in the ferrite matrix. Austenite forms on cementite particles located on grain boundaries. The steel microstructure at $T = Ac1$ can thus be represented by a simulation cell with a spherical geometry (**Figure 1 (b)**). A cementite particle of initial radius R_θ is embedded in a ferrite shell of thickness L_α .

As determined by ICP-MS on a sample heated up to 700°C at 1°C/s, cementite initial Mn and Cr enrichment is of 14.1 wt.% Mn and 2.9 wt.% Cr. This mean chemistry is compared to the orthoequilibrium chemistry of cementite calculated by Thermo-Calc when a ferrite-cementite equilibrium is forced up to 710°C (i.e. austenite presence is forbidden) (**Figure 2**). Since both chemistries differ significantly and the effects of w_{Mn}^θ and w_{Cr}^θ on austenite formation kinetics are not known, the orthoequilibrium one cannot be used as initial set-up conditions.

Since carbon is a fast-diffusing element, it can be assumed that cementite equilibrium volume fraction $f_{v,eq}^\theta$ has been reached far before $T = Ae1$. This fraction is calculated with Thermo-Calc. Mean initial radius of cementite is determined from image analysis with Fiji software [28] from FEG-SEM micrographs and found to be about 50 nanometers. Lastly, the thickness of ferrite shell L_α is adjusted in respect to $f_{v,eq}^\theta$, and ferrite chemistry is derived from the nominal chemistry by a mass balance.

Calculations are started from $T = Ae1 = 642^\circ C$ to ensure that no absurd transformation kinetics are obtained between $T = Ae1$ and $T = Ac1$.

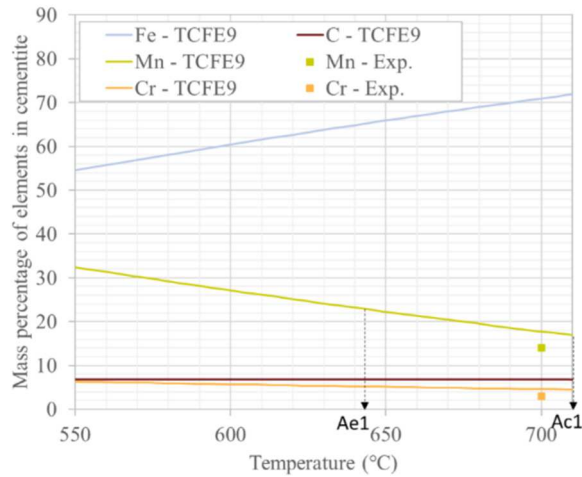


Figure 2 – Calculated chemistry for cementite with Thermo-Calc (TCFE9 database) under forced $\alpha - \theta$ equilibrium up to 710°C, and initial chemistry of cementite as measured by ICP mass spectrometry (1°C/s heating up to 700°C).

3.1. FeCMn system

Calculations were first carried out in the ternary FeCMn system. As a first guess, it is hereby assumed that Cr effects on austenite formation kinetics can be neglected, as it is only a minor element in the steel chemistry when compared to Mn or Si. Ae1 and Ae3 temperatures of this system are given in **Table 2**. Initial phases chemistries can be found in **Table 3**.

Table 2 – Remarkable temperatures of considered FeCMn and FeCMnCr systems calculated with Thermo-Calc (TCFE9 database).

[°C]	Fe-C-2.57Mn	Fe-C-2.57Mn-0.31Cr
Ae1	645	648
Ae3	769	767

Table 3 – Initial DICTRA conditions at T = Ae1 for the Fe-C-2.57Mn system.

[wt.%]	C	Mn	Cr	f_{eq}
α	3.6×10^{-3}	2.2	-	97.01 vol.%
θ	6.72	14.1	-	2.99 vol.%

The evolution of elemental composition gradients and activities in phases are checked during heating to help understand how the simulation cell undergoes austenite formation (**Figure 3 (a) to (d)**). The θ/γ interface will not be considered in this study, since austenitization mainly progresses thanks to the transformation of α into γ . Thus, austenite formation will be explained by the evolutions of composition gradients and activities in α and γ only.

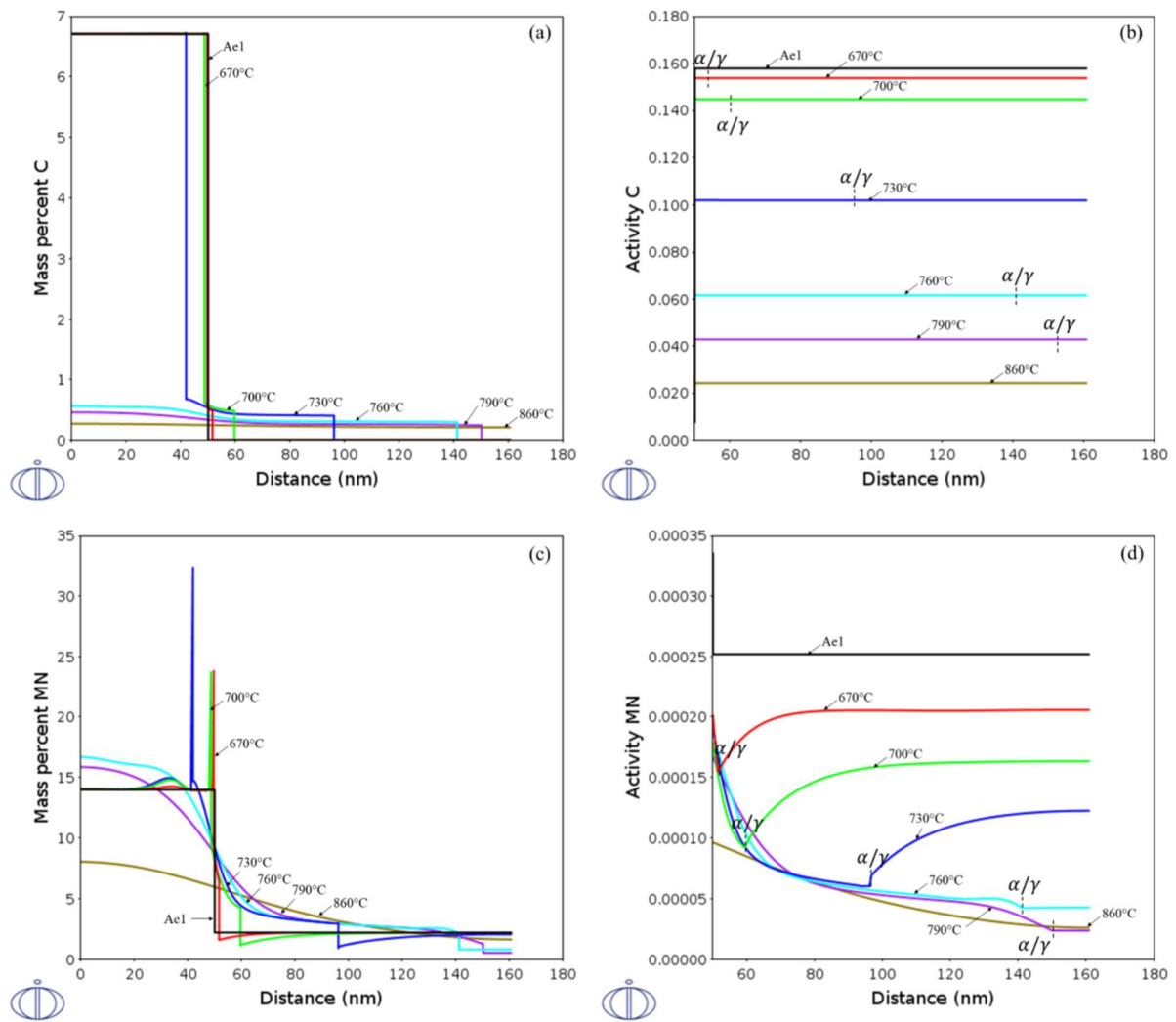


Figure 3 – Composition (a,c) and activity (b,d) profiles of C and Mn during heating as calculated by DICTRA. Position of α/γ interface at each temperature is given by the dashed lines in the activity diagrams.

The absence of a C gradient in ferrite and the flatness of its activity profile (**Figure 3 (a,b)**) in both austenite and ferrite at all temperatures confirm that this element cannot be held responsible for austenite formation kinetics. This result was anticipated, as carbon diffusivity is much higher than Mn diffusivity at all considered temperatures.

Between Ae1 and 730°C, a very distinct gradient of Mn activity in ferrite near the austenite-ferrite transformation interface can be seen (**Figure 3 (d)**). This indicates Mn diffusion towards growing austenite. This is confirmed by the Mn composition gradient in ferrite in this temperature interval (**Figure 3 (c)**). For temperatures above 760°C, Mn activity has been homogenized in ferrite and no composition gradient can be detected anymore between the α/γ interface and the outer boundary. Mn diffusivity is now high enough to almost instantly equalize its activity in ferrite. However, an activity gradient is still very clearly visible in austenite. As Mn diffuses slower in austenite than ferrite, diffusion did not erase the composition gradient built from cementite dissolution, and austenite formation is now controlled by Mn diffusion in that phase. At $T = 860^\circ\text{C}$, Mn activity profile and

composition gradients are less marked but are not flat. Orthoequilibrium is thus not reached yet, even though the whole simulation cell is transformed into austenite.

In these anisothermal conditions, austenite transformation appears to follow the classical scheme already reported for isothermal holdings [6]. The first stage of the transformation kinetics is controlled by Mn diffusion in ferrite, and the second stage by Mn diffusion in austenite, up until orthoequilibrium is reached. This final equilibrium could in this study be obtained by heating to higher temperatures or by holding at final temperature for some time.

However, simulated austenite formation kinetics in the FeCMn system does not agree well with the experimental kinetics determined by dilatometry (**Figure 5**). New simulations considering the presence of chromium were thus carried out to represent more accurately the austenitization conditions of the studied steel. It has indeed already been reported that the addition of 1 wt.% of Cr can make the austenitization kinetics very sluggish [8,17]. We can thus expect the kinetics to be altered by the addition of 0.31 wt.% Cr in the calculations.

3.2. FeCMnCr system

A similar analysis to the one made for the FeCMn system was conducted for the FeCMnCr system. Ae1 and Ae3 temperatures of this system are given in **Table 2** and initial phase compositions of ferrite and cementite are given in **Table 4**. Composition and activity profiles were checked at several temperatures during heating (**Figure 6 (a) to (e)**). Just like the FeCMn case, C activity in austenite and ferrite equalizes rapidly. Once again, C is not responsible for the global austenitization kinetics. Small composition gradients of C can be seen in austenite throughout heating: they are the consequence of the flux coupling with Mn and Cr composition gradients due to the attractive Mn-C and Cr-C interactions.

Table 4 – Initial DICTRA conditions at T = Ae1 for the Fe-C-2.57Mn-0.31Cr system.

[wt.%]	C	Mn	Cr	f_{eq}
α	3.3×10^{-3}	2.22	0.22	97 vol.%
θ	6.72	14.1	2.85	3 vol.%

Figure 6 (c,e) and **Figure 6 (d,f)** respectively show Mn and Cr composition and activity profiles during austenite growth for several temperatures. When temperatures are below 760°C, a clear activity gradient in ferrite can be seen for both elements. As composition gradients exist in ferrite at these same temperatures, this indicates that austenite growth is first controlled by Mn or Cr diffusion in ferrite towards austenite. C, Mn and Cr diffusion coefficients in ferrite and austenite are given in **Figure 4**. As D_{Mn} and D_{Cr} are very close to each other in the investigated temperature range, one cannot discriminate their individual effects on austenite formation kinetics.

For temperatures above 790°C, Mn and Cr activities seem to have become homogeneous in ferrite. This would indicate that D_{Mn}^α and D_{Cr}^α are now sufficiently high to “erase” composition and activity gradients in ferrite, and that Mn and Cr diffusion in ferrite do not control the transformation kinetics anymore.

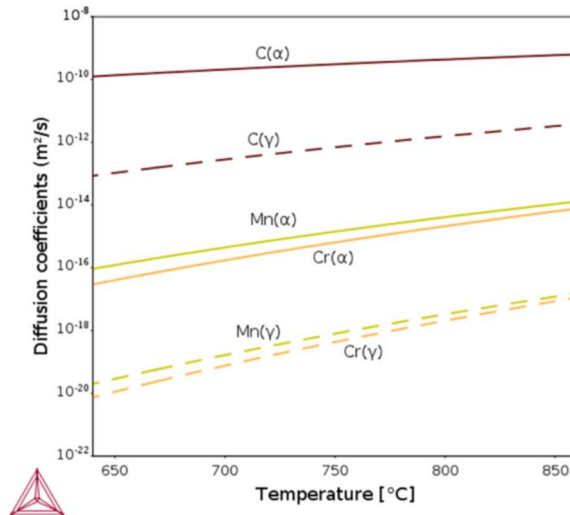


Figure 4 - Diffusion coefficients (in m²/s) of C, Mn and Cr in ferrite and austenite as calculated by Thermo-Calc with TCFE9 and MOB2 databases.

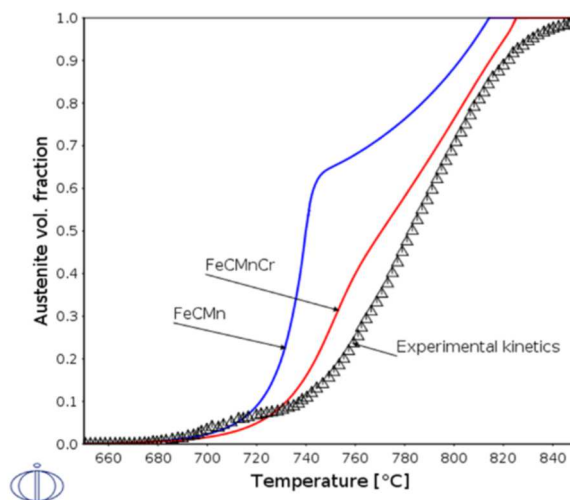


Figure 5 – Comparison of simulated (FeCMn system) and experimental austenite formation kinetics (by dilatometry).

In austenite, below 760°C, very steep gradients of activity and composition exist. Diffusivities are not high enough to erase these gradients. Above 790°C, however, there is an on-going process of austenite homogenization during its growth, as can be seen by the progressive flattening of activity profiles in austenite (**Figure 6 (d,f)**). Therefore, it seems that austenite formation is now controlled by Mn and Cr diffusion in austenite until full orthoequilibrium is reached. Thus, Cr presence does not seem to change the austenite growth mode (compared to FeCMn system). However, as shown in **Figure 5**, austenite formation kinetics is deeply modified by Cr addition. A reasonable agreement between simulated and experimental kinetics is now found. **It is necessary to understand why Cr shows such a**

delaying effect on the transformation kinetics, and why the kinetics of the FeCMnCr case do not show a sharp transition like the one observed for the FeCMn case.

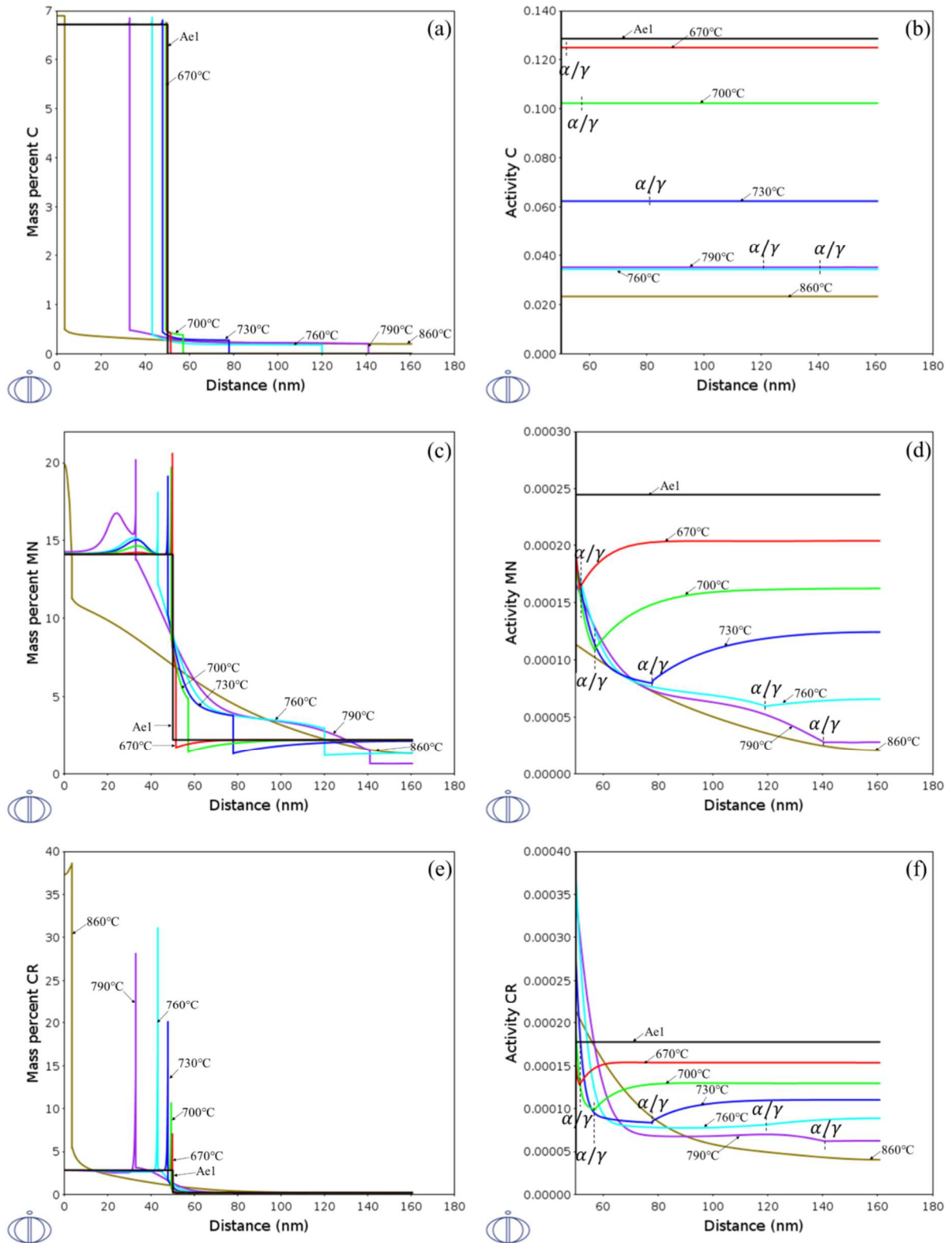


Figure 6 – Composition (a,c,e) and activity (b,d,f) profiles of C, Mn and Cr during heating as calculated by DICTRA. Position of α/γ interface at each temperature is given by the dashed lines in the activity diagrams.

3.3. Origin of Cr delaying effect on austenite formation kinetics

A first explanation for the delaying effect of Cr addition on austenite formation kinetics simply lies on a slightly higher Ae1 temperature (+3°C) for the +Cr-case (**Table 2**). It can be noted that this evolution is partly due to a greater stability of cementite, as it is now Cr-enriched ($G_m^\theta(FeCMn) = -36,5 \text{ kJ}\cdot\text{mol}^{-1}$ and $G_m^\theta(FeCMnCr) = -37,9 \text{ kJ}\cdot\text{mol}^{-1}$ at 640°C, with 5.2 wt.% Cr in θ). This difference is however not enough to explain why both kinetics is so different in each case.

The evolution of the Gibbs energy dissipation rate is obtained by full equilibrium calculations (**Figure 7**). It is defined as $\frac{\partial G_m^{tot}}{\partial t} = H_R \cdot \frac{\partial G_m^{tot}}{\partial T}$, with G_m^{tot} being the total molar Gibbs energy of the simulation cell and H_R the heating rate. As the heating rate is of 1°C/s in the present case, $\frac{\partial G_m^{tot}}{\partial t}$ can thus simply be calculated with Thermo-Calc. However, it does not help to explain austenite formation kinetics. Indeed, both $\Delta G_{diss}^Y(FeCMn)$ and $\Delta G_{diss}^Y(FeCMnCr)$ are very close to each other between 640°C and 860°C. Moreover, $\Delta G_{diss}^Y(FeCMnCr)$ is even slightly lower than $\Delta G_{diss}^Y(FeCMn)$, which is not compatible with the calculated austenitization kinetics. Another explanation must be found to understand why Cr changes the austenitization kinetics so much.

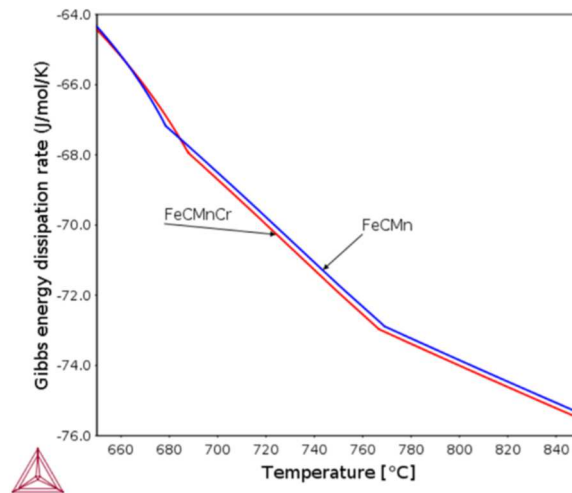


Figure 7 – Evolution of the Gibbs energy dissipation rate for both FeCMn and +Cr cases.

The velocity of the α/γ interface is proportional to the flux difference at this interface (“entering” minus “leaving” fluxes). To understand how Cr addition slows down the transformation kinetics, we considered the evolution of $\Delta J_{Mn} = J_{Mn}^{\gamma/\alpha} - J_{Mn}^{\alpha/\gamma}$, with $J_{Mn}^{\gamma/\alpha} > 0$ and $J_{Mn}^{\alpha/\gamma} < 0$. **Figure 8 (a)** and **(b)** give the evolutions of ΔJ_{Mn} and $v_{\alpha/\gamma}$ with temperature. The ΔJ_{Mn} curves are classical C-curves, whose intensities are the result of simultaneous evolution of diffusivities and composition gradients. Since it is known that Mn/Cr diffusivities rise with temperature (**Figure 4**), we will take special interest in the evolution of composition gradients through the study of appropriate phase diagrams.

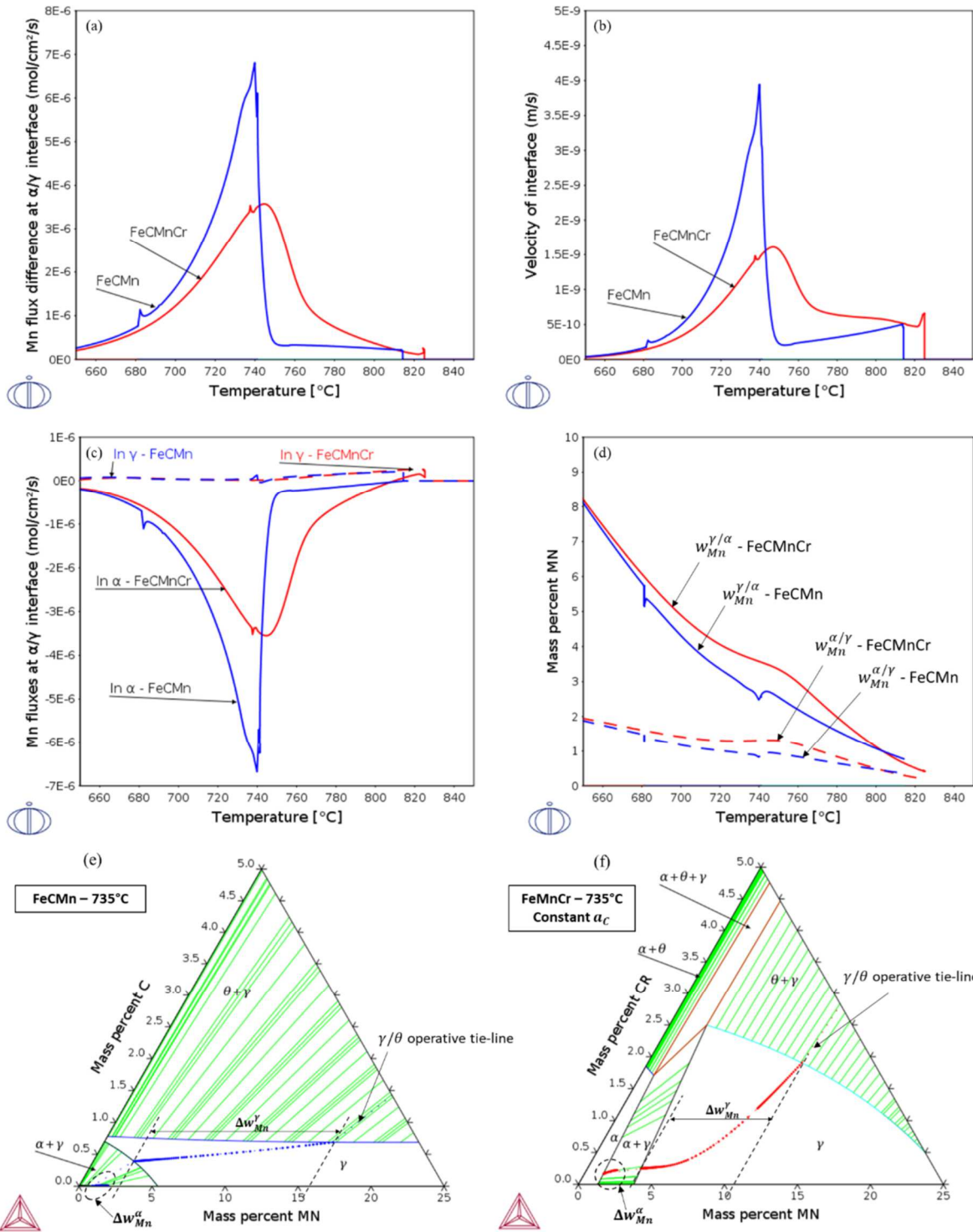


Figure 8 – (a) Evolution of Mn flux difference ΔJ_{Mn} at α/γ interface with temperature; (b) Velocity of α/γ interface with temperature; (c) Evolution of Mn fluxes on both sides of α/γ interface with temperature; (d) Evolution of interfacial compositions on α/γ interface with temperature; (e) Partial FeCMn phase diagram at 735°C (zoom on the γ domain) ; (f) Pseudo-ternary FeMnCr phase diagram (zoom on the γ domain) at constant carbon activity. Corresponding diffusion paths are drawn in dotted curves.

In a phase diagram, the interfacial compositions chosen to respect local equilibrium at an interface are given by the operative tie-lines. Therefore, composition gradients in each phase result from the positions of these tie-lines and their evolutions with temperature. It would be complex and tedious to analyze diffusion paths in each phase diagram at each temperature. According to **Figure 8 (a)** and **(b)**, Cr affects transformation kinetics the most at around 735°C. Indeed, Mn flux difference on α/γ interface is strongly diminished by Cr addition on the whole temperature range, but especially at this temperature. Individual fluxes must be looked at to understand this behavior.

Figure 8 (c) shows the evolutions of Mn fluxes in ferrite and austenite on the α/γ interface with temperature. For the FeCMn case, it is obvious from **Figure 8 (a)** and **(c)** that for temperatures below 740°C, $\Delta J_{Mn} \approx -J_{Mn}^{\alpha/\gamma}$, which means that for these temperatures the transformation kinetics is controlled by diffusion in ferrite. Between 740°C and 750°C, $J_{Mn}^{\alpha/\gamma}$ drops as diffusivities become high enough to equalize the existing composition gradients in ferrite. Then, above 750°C, $\Delta J_{Mn} \approx J_{Mn}^{\gamma/\alpha}$, showing that diffusion in austenite now controls the transformation kinetics. A sudden growth mode transition has thus been happening between 740°C and 750°C, hence the observed two-step kinetics.

The scenario is different in the +Cr-case. **Figure 8 (a)** and **(c)** show that diffusion in ferrite controls the transformation kinetics up to around 800°C, as $\Delta J_{Mn} \approx -J_{Mn}^{\alpha/\gamma}$ below this temperature. Only then does diffusion in austenite become dominant ($\Delta J_{Mn} \approx J_{Mn}^{\gamma/\alpha}$). Two conclusions can thus be drawn about Cr effect. On one hand, its addition does not change the austenite growth mode, which still sees a transition between diffusion in ferrite and austenite being the kinetically controlling mechanism. On the other hand, Cr has been affecting Mn flux in ferrite such that the growth mode transition still begins around 740°C (when $J_{Mn}^{\alpha/\gamma}$ starts to decrease) but ends much later (800°C). Since $J_{Mn}^{\alpha/\gamma}$ fades more progressively in the +Cr-case than in the FeCMn case, the transformation kinetics lose their two-step character and become smoother.

Then, the delaying effect of Cr on the transformation can be understood with the evolution of interfacial compositions on α/γ interface (**Figure 8 (d)**). Considering the FeCMn case, no sudden change in $w_{Mn}^{\alpha/\gamma}$ can be seen between 740°C and 750°C. This indicates that the growth mode transition does not originate from specific interfacial conditions but indeed from the rise of diffusivities with temperature, progressively erasing the composition gradient Δw_{Mn}^{α} in ferrite. For the +Cr-case, $w_{Mn}^{\alpha/\gamma}$ is increased on the whole investigated temperature range. Therefore, $\Delta w_{Mn}^{\alpha}(FeCMnCr) < \Delta w_{Mn}^{\alpha}(FeCMn)$ and $J_{Mn}^{\alpha/\gamma}$ is weaker. This implies a slower movement of the transformation interface (**Figure 8 (b)**) and, in the end, delayed transformation kinetics.

Finally, it is interesting to look at the phase diagrams of the FeCMn and FeCMnCr systems. They are plotted at 735°C in **Figure 8 (e)** and **(f)**. For the FeCMnCr case, this diagram is plotted at constant carbon activity, as it has been seen that C activity was uniform between ferrite and austenite (**Figure 6 (b)**). It is seen with these diagrams that Cr consideration mostly affects Δw_{Mn}^{γ} , which is done by having a strong decreasing influence on $w_{Mn}^{\gamma/\theta}$. However, since diffusivities are much lower in austenite than ferrite, $J_{Mn}^{\gamma/\alpha}$ does not

vary much and stays low (**Figure 8 (c)**). In ferrite, Δw_{Mn}^{α} does not seem to be strongly altered by Cr addition. Yet, the combination of this small gradient change with high diffusivities in this phase result in a strong variation of Mn flux, as explained previously.

3.4. Expected effect of silicon

This study was led without considering silicon, as there is no available mobility data for this element in cementite in MOB2 database. Yet, it is a major constituent of the studied steel. It has to be noted that adding 0.9 wt.% Si in the Thermo-Calc calculations increases Ae1 by $\sim 15^{\circ}\text{C}$. This increase is approximately the temperature discrepancy between the calculated and experimental kinetics (FeCMnCr case, **Figure 5**). **Taking Si into account thus might help to optimize the agreement between the calculations and experience.** Following that silicon is a ferrite-stabilizer element, Mn interfacial composition in ferrite is expected to be higher with Si consideration. This would reduce Δw_{Mn}^{α} and lead to another delay in the transformation kinetics.

3.5. Cementite size and chemistry

Three parameters are considered to characterize cementite before austenite formation: its mean radius, Mn enrichment and Cr enrichment. Each parameter was varied individually to observe its influence on austenite formation kinetics. The steel nominal chemistry was kept constant.

For the sake of simplicity, and to prevent the inclusion of too many images in this paper, only one phase diagram will be presented for each varied parameter in the next sections. The diffusion paths of each case will be drawn on this diagram. It is plotted at 735°C with constant carbon activity. The chosen value for a_c is the one seen at the α/γ interface for the case previously discussed (for which $w_{Mn}^{\theta} = 14.1$ wt.% and $w_{Cr}^{\theta} = 2.9$ wt.%). Therefore, the diffusion paths of other cases do not perfectly superimpose with the diagram.

3.5.1. Effect of cementite Mn initial content

As the nominal chemical composition is fixed, a Mn enrichment of cementite w_{Mn}^{θ} implies that the surrounding ferrite is depleted in Mn (**Table 5**). Mn enrichment is varied from an arbitrarily low level of 10 wt.% to the orthoequilibrium one (22.7 wt.%), calculated by Thermo-Calc at a temperature just below Ae1.

Table 5 – Evolution of initial ferrite Mn content with cementite Mn enrichment (in wt.%).

w_{Mn}^{θ}	10	14	18	22.7
w_{Mn}^{α}	2.35	2.22	2.11	1.96

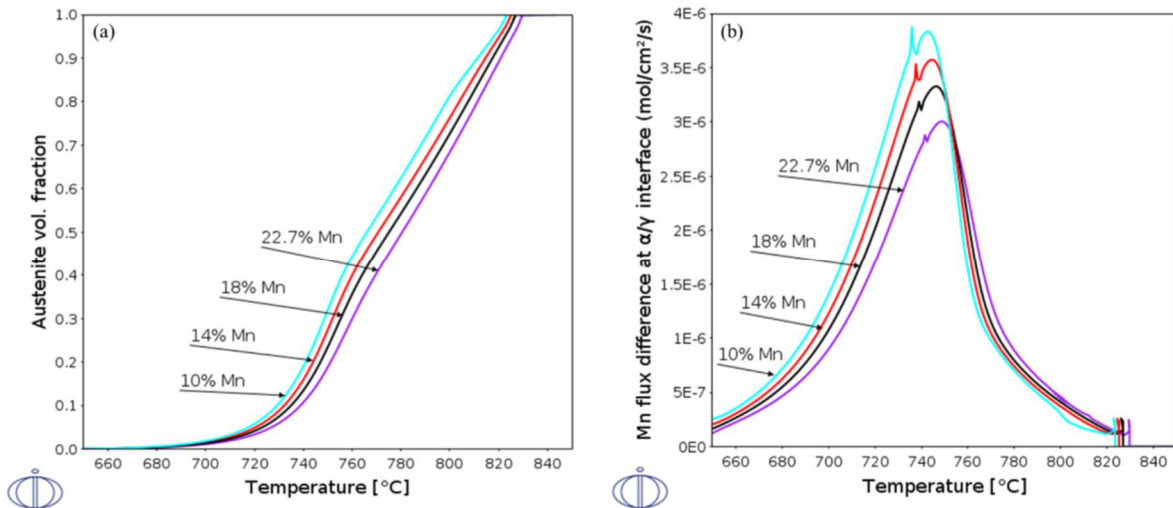


Figure 9 – (a) Effect of initial cementite Mn enrichment on austenite formation kinetics during 1°C/s heating; (b) Mn flux difference seen at the α/γ interface.

Austenite transformation is simulated for 4 different values of w_{Mn}^θ . An enriched particle delays the transformation to higher temperatures (**Figure 9 (a)**). The evolution of ΔJ_{Mn} with temperature for each level of cementite enrichment is given in **Figure 9 (b)**. Diffusion paths are given on the phase diagram at 735°C in **Figure 10 (a)** and **(b)** (zoom on the $\alpha + \gamma$ domain).

It appears that higher values of w_{Mn}^θ not only lead to a reduced mean Mn content in ferrite, but also slightly diminish $w_{Mn}^{\alpha/\gamma}$ values (**Figure 10 (b)**). Overall, Δw_{Mn}^α becomes lower for higher Mn cementite content since the decrease of $w_{Mn}^{\alpha/\gamma}$ is lower than that of $w_{Mn}^{\alpha,ext}$. As a result, since it is known that $J_{Mn}^{\alpha/\gamma}$ is dominant for most of the transformation, the velocity of the transformation interface decreases. Thus, transformation kinetics is delayed to higher temperatures when cementite Mn content is increased.

Varying w_{Mn}^θ from 10 to 22.7 wt.% delays the austenite formation kinetics of approximately 15°C at $f_\gamma = 0.5$. This delay is rather important, as it takes about 90°C in each case to go from $f_\gamma = 0.1$ to $f_\gamma = 0.9$. Mn initial cementite enrichment thus appears as an important parameter regarding austenitization kinetics and should not be neglected.

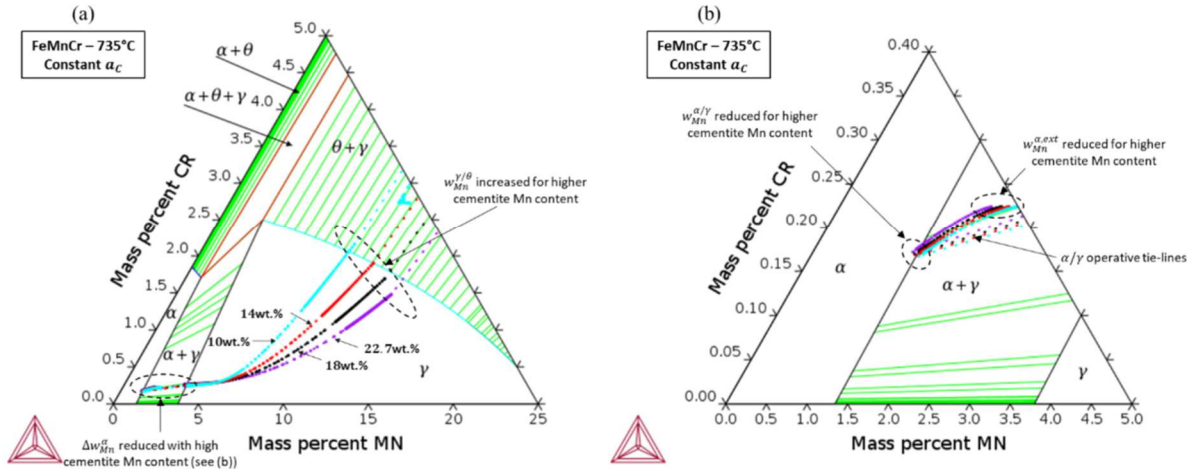


Figure 10 – (a) Pseudo-ternary FeMnCr phase diagram at 735°C (zoom on the γ domain) at constant carbon activity. Diffusion paths of each case are drawn. Slight deviations from the $\gamma/\gamma + \theta$ frontier occur due to different values of carbon activity at 735°C for each Mn content of cementite; (b) Zoom on the $\alpha + \gamma$ domain.

3.5.2. Effect of cementite Cr initial content

Similarly to the previous case, increasing w_{Cr}^θ implies that ferrite is depleted in Cr, as nominal composition is fixed (Table 6). Cr enrichment was varied from 2 wt.% to 5.2 wt.%, which is the orthoequilibrium enrichment calculated by Thermo-Calc at a temperature just below Ae1.

Table 6 - Evolution of initial ferrite Cr content with cementite Cr enrichment (in wt.%)

w_{Cr}^θ	2	2.9	4	5.2
w_{Cr}^α	0.25	0.22	0.19	0.15

Following Figure 11 (a), similarly to Mn effect, increasing cementite Cr content delays the transformation kinetics to higher temperatures. Indeed, ΔJ_{Mn} is slightly decreased, thus slowing down the corresponding transformation kinetics (Figure 11 (b)). The diffusion paths in Figure 12 (b) show that when increasing Cr content, $w_{Mn}^{\alpha/\gamma}$ is also slightly increased. Consequently, as $w_{Mn}^{\alpha,ext}$ is not affected by Cr initial distribution, Δw_{Mn}^α becomes lower when w_{Cr}^θ is increased. Finally, the transformation kinetics is slowed down, as they are primarily decided by $J_{Mn}^{\alpha/\gamma}$ evolution.

Like Mn, the effect of cementite Cr enrichment on transformation kinetics is also rather important. The delay is of about 15°C at $f_\gamma = 0.5$ when increasing w_{Cr}^θ from 2 wt.% to 5.2 wt.%.

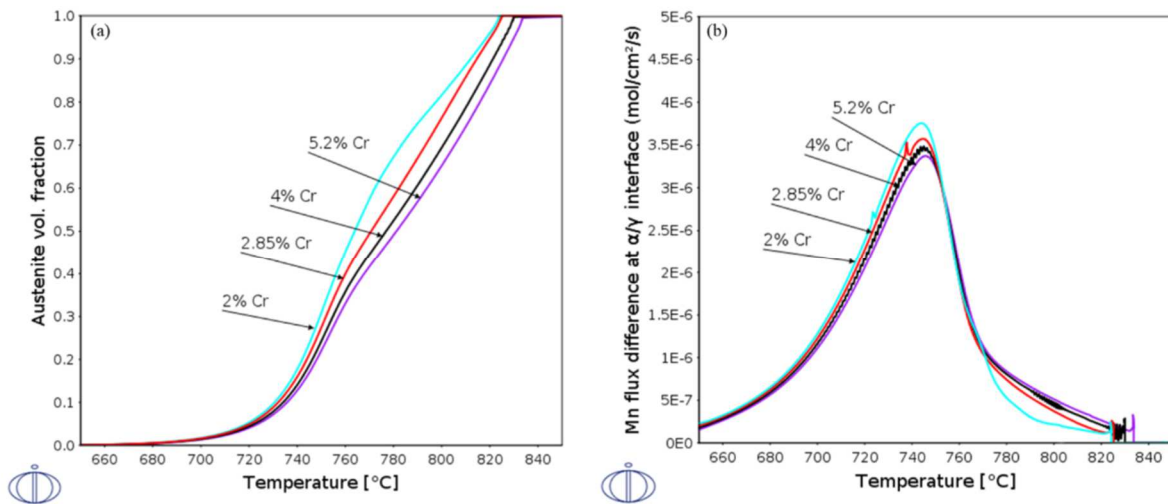


Figure 11 – (a) Effect of initial cementite Cr enrichment on austenite formation kinetics during 1°C/s heating; (b) Mn flux difference seen at α/γ interface.

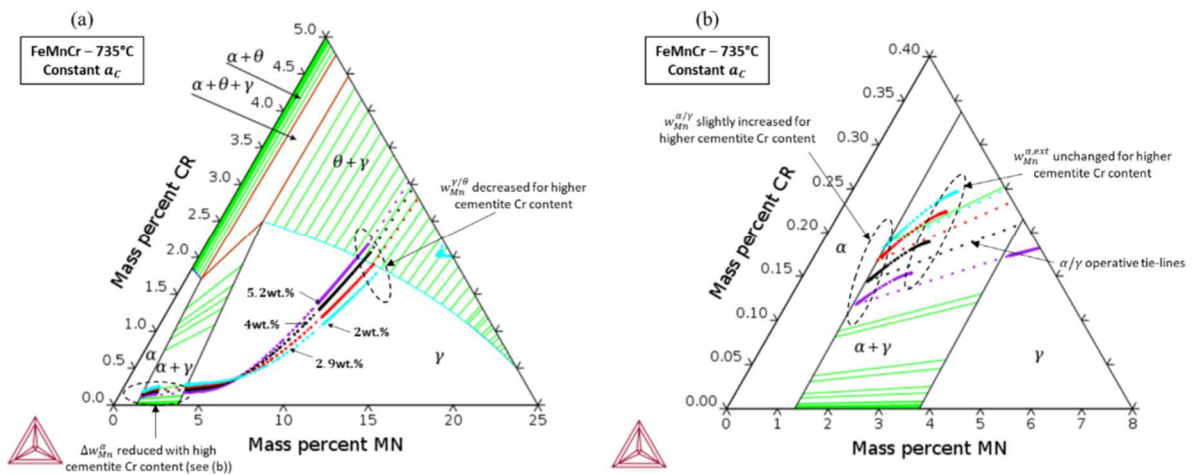


Figure 12 - (a) Pseudo-ternary FeMnCr phase diagram at 735°C (zoom on the γ domain) at constant carbon activity; (b) Zoom on the $\alpha + \gamma$ domain.

3.5.3. Effect of cementite initial radius

The main consequence of a R_θ variation is the modification of the total size of the simulation cell. Volume fraction of cementite is fixed: increasing R_θ results in an increase of the ferrite shell thickness. Distances on which elements must diffuse to assist the austenitic transformation are therefore increased, and transformation kinetics will inevitably be delayed by the increase of this parameter, as “more matter” has to be transformed into austenite.

Austenite formation kinetics is deeply altered by a change in R_θ (Figure 13 (b)). Maximum intensity for ΔJ_{Mn} is reached at around 710°C for $R_\theta = 20$ nm, 740°C for 50 nm (reference case) and 770°C for 80 nm. This variation is a direct consequence of the simulation cell size: the smaller initial cementite radius, the smaller distance Mn must cross in ferrite to equalize its composition gradient. Therefore, diffusivities do not need to be particularly high

to see this gradient being progressively erased, hence the lower temperature at which ΔJ_{Mn} sees its maximum intensity.

For bigger particles ($R_\theta = 80$ nm), increasing f_γ of the same amount than for small particles asks for the transformation interface to travel on a larger distance. For that reason, the corresponding transformation kinetics seem to take more time to “start” than for small particles. Temperature has to be increased more than for small particles to start erasing the composition gradient in ferrite. This is related to the transformation interface having to go further to get close to the outer boundary of the simulation cell. This combination of a very high diffusivity (higher temperature) to a still important gradient in ferrite leads to a high maximum intensity for $J_{Mn}^{\alpha/\gamma}$ and, consequently, for ΔJ_{Mn} .

In isothermal cases, increasing the initial radius would lead to a delay in time with a R^2 dependence, as the diffusion distance is expressed as $L^2 = D_{Mn}t$. However, in anisothermal conditions, D_{Mn} becomes a function of temperature. This implies that increasing the cementite initial radius leads to a delay in time with a $R^2/D_{Mn}(T)$ dependence. During heating, the delay progressively decreases as $D_{Mn}(T)$ also increases. Finally, the transformation kinetics seen for “big-particle kinetics” catch up on the “small-particle kinetics” at high temperatures.

It is noteworthy that since the cementite volume fraction is kept constant, increasing its initial radius is the numerical equivalent to, experimentally, a decrease in austenite nuclei density. What matters most is not the absolute value of cementite radius but the ferrite volume that then needs to be transformed to complete the transformation. This is why cementite radius is such an influential parameter on the transformation kinetics.

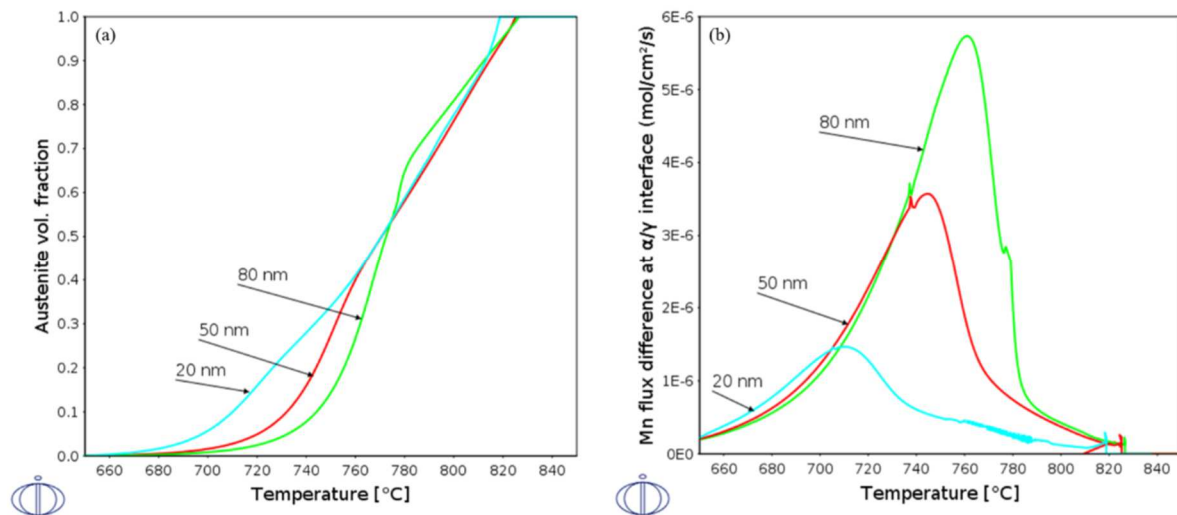


Figure 13 – (a) Effect of cementite initial radius on austenite formation kinetics; (b) Mn flux difference seen at α/γ interface.

For larger particles, due to the longer time needed to see the “effective start” of the transformation and the effect of the $R^2/D_{Mn}(T)$ dependence, the resulting kinetics are non-

monotonous (accelerating and decelerating stages). Therefore, most of the transformation spans on a tighter temperature range than small-particle kinetics, which are more regular. As a result, large particles might be detrimental to a good control of the transformed austenite fraction upon heating. However, thermomechanical treatments needed to obtain smaller particles in the microstructure might lead to other microstructural transformations that could themselves have other effects on the transformation kinetics.

4. Summary

It has been shown in this study that Cr plays an important role on austenite formation kinetics during heating, as it modifies Mn fluxes in ferrite by changing the positions of operative tie-lines during the transformation, resulting in a weaker Mn flux difference at the transformation interface. Transformation kinetics is thus delayed to higher temperatures. Reasonable agreement between simulated and experimental kinetics can only be obtained if Cr is considered in the calculations.

Three parameters used to characterize cementite before austenite formation (Mn/Cr enrichment, initial radius) have been individually varied to study their effects on austenite formation kinetics during heating. It was shown that Mn and Cr enrichment levels have a relatively high influence on the transformation kinetics (delay of approximately 15°C for w_{Mn}^{θ} from 10 to 22.7 wt.% or w_{Cr}^{θ} from 2 to 5.2 wt.%). Thus, cementite chemistry should be properly considered to accurately predict austenite formation kinetics. Moreover, cementite initial radius is the most influential parameter, leading to dramatic changes on the transformation kinetics. This effect is related to the equivalent change of austenite nuclei density.

Acknowledgements

This project was supported by the National Association of Research and Technology (ANRT – Project n°2017/0799).

Data availability

The raw/processed data required to reproduce these findings can be obtained by contacting the corresponding author.

References

- [1] N. Fonstein, Advanced high strength sheet steels: physical metallurgy, design, processing, and properties, Springer, 2015.
- [2] O. Bouaziz, H. Zurob, M. Huang, Driving force and logic of development of Advanced High Strength Steels for automotive applications, Steel Research International. (2013) 937–947. <https://doi.org/10.1002/srin.201200288>.

- [3] D. Bhattacharya, Microalloyed steels for the automotive industry, *Tecnologia Em Metalurgia Materiais e Mineração*. 11 (2014) 371–383. <https://doi.org/10.4322/tmm.2014.052>.
- [4] C. Philippot, J. Drillet, P. Maugis, V. Hebert, M. Dumont, Austenite formation in a ferrite/martensite cold-rolled microstructure during annealing of advanced high-strength steels, *Metall. Res. Technol.* 111 (2014) 3–8. <https://doi.org/10.1051/metal/2014004>.
- [5] M. Bellavoine, M. Dumont, J. Drillet, V. Hébert, P. Maugis, Combined effect of heating rate and microalloying elements on recrystallization during annealing of dual-phase steels, *Metallurgical and Materials Transactions A*. 49 (2018) 2865–2875. <https://doi.org/10.1007/s11661-018-4642-z>.
- [6] G.R. Speich, V.A. Demarest, R.L. Miller, Formation of austenite during intercritical annealing of dual-phase steels, *Metallurgical and Materials Transactions A*. 12 (1981) 1419–1428. <https://doi.org/10.1007/BF02643686>.
- [7] J. Huang, W.J. Poole, M. Militzer, Austenite formation during intercritical annealing, *Metallurgical and Materials Transactions A*. 35 (2004) 3363–3375. <https://doi.org/10.1007/s11661-004-0173-x>.
- [8] G. Miyamoto, H. Usuki, T. Furuhashi, Effects of Mn, Si and Cr addition on reverse transformation at 1073K from spheroidized cementite structure in Fe–0.6 mass% C alloy, *Acta Materialia*. 58 (2010) 4492–4502. <https://doi.org/10.1016/j.actamat.2010.04.045>.
- [9] H. Azizi-Alizamini, M. Militzer, W.J. Poole, Austenite formation in plain low-carbon steels, *Metallurgical and Materials Transactions A*. 42 (2011) 1544–1557. <https://doi.org/10.1007/s11661-010-0551-5>.
- [10] R. Wei, M. Enomoto, R. Hadian, H.S. Zurob, G.R. Purdy, Growth of austenite from as-quenched martensite during intercritical annealing in an Fe–0.1C–3Mn–1.5Si alloy, *Acta Materialia*. 61 (2013) 697–707. <https://doi.org/10.1016/j.actamat.2012.10.019>.
- [11] Y. Xia, M. Enomoto, Z. Yang, Z. Li, C. Zhang, Effects of alloying elements on the kinetics of austenitization from pearlite in Fe–C–M alloys, *Philosophical Magazine*. 93 (2013) 1095–1109. <https://doi.org/10.1080/14786435.2012.744484>.
- [12] Q. Lai, M. Gouné, A. Perlade, T. Pardoën, P. Jacques, O. Bouaziz, Y. Bréchet, Mechanism of austenite formation from spheroidized microstructure in an intermediate Fe-0.1C-3.5Mn steel, *Metallurgical and Materials Transactions A*. 47 (2016) 3375–3386. <https://doi.org/10.1007/s11661-016-3547-y>.
- [13] Z.N. Yang, M. Enomoto, C. Zhang, Z.G. Yang, Transition between alloy–element partitioned and non-partitioned growth of austenite from a ferrite and cementite mixture in a high-carbon low-alloy steel, *Philosophical Magazine Letters*. 96 (2016) 256–264. <https://doi.org/10.1080/09500839.2016.1197432>.
- [14] M. Enomoto, S. Li, Z.N. Yang, C. Zhang, Z.G. Yang, Partition and non-partition transition of austenite growth from a ferrite and cementite mixture in hypo- and hypereutectoid Fe-C-Mn alloys, *Calphad*. 61 (2018) 116–125. <https://doi.org/10.1016/j.calphad.2018.03.002>.
- [15] X. Zhang, G. Miyamoto, T. Kaneshita, Y. Yoshida, Y. Toji, T. Furuhashi, Growth mode of austenite during reversion from martensite in Fe-2Mn-1.5Si-0.3C alloy: A transition in kinetics and morphology, *Acta Materialia*. 154 (2018) 1–13. <https://doi.org/10.1016/j.actamat.2018.05.035>.
- [16] M. Ollat, M. Militzer, V. Massardier, D. Fabregue, E. Buscarlet, F. Keovilay, M. Perez, Mixed-mode model for ferrite-to-austenite phase transformation in dual-phase steel, *Computational Materials Science*. 149 (2018) 282–290. <https://doi.org/10.1016/j.commatsci.2018.02.052>.

- [17] Z.-D. Li, G. Miyamoto, Z.-G. Yang, T. Furuhashi, Kinetics of reverse transformation from pearlite to austenite in an Fe-0.6 mass pct C alloy and the effects of alloying elements, *Metallurgical and Materials Transactions A*. 42 (2011) 1586–1596. <https://doi.org/10.1007/s11661-010-0560-4>.
- [18] M. Gouné, P. Maugis, J. Drillet, A criterion for the change from fast to slow regime of cementite dissolution in Fe–C–Mn steels, *Journal of Materials Science & Technology*. 28 (2012) 728–736. [https://doi.org/10.1016/S1005-0302\(12\)60122-4](https://doi.org/10.1016/S1005-0302(12)60122-4).
- [19] M. Enomoto, K. Hayashi, Simulation of the growth of austenite during continuous heating in low carbon iron alloys, *Journal of Materials Science*. 50 (2015) 6786–6793. <https://doi.org/10.1007/s10853-015-9234-3>.
- [20] M. Enomoto, K. Hayashi, Modeling the growth of austenite in association with cementite during continuous heating in low-carbon martensite, *Journal of Materials Science*. 53 (2018) 6911. <https://doi.org/10.1007/s10853-018-2020-2>.
- [21] F.M. Castro Cerda, I. Sabirov, C. Goulas, J. Sietsma, A. Monsalve, R.H. Petrov, Austenite formation in 0.2% C and 0.45% C steels under conventional and ultrafast heating, *Materials & Design*. 116 (2017) 448–460. <https://doi.org/10.1016/j.matdes.2016.12.009>.
- [22] G. Liu, Z. Dai, Z. Yang, C. Zhang, J. Li, H. Chen, Kinetic transitions and Mn partitioning during austenite growth from a mixture of partitioned cementite and ferrite: Role of heating rate, *Journal of Materials Science & Technology*. 49 (2020) 70–80. <https://doi.org/10.1016/j.jmst.2020.01.051>.
- [23] R. Wei, M. Enomoto, R. Hadian, H.S. Zurob, G.R. Purdy, Growth of austenite from as-quenched martensite during intercritical annealing in an Fe–0.1C–3Mn–1.5Si alloy, *Acta Materialia*. 61 (2013) 697–707. <https://doi.org/10.1016/j.actamat.2012.10.019>.
- [24] J. Emo, P. Maugis, A. Perlade, Austenite growth and stability in medium Mn, medium Al Fe-C-Mn-Al steels, *Computational Materials Science*. 125 (2016) 206–217. <https://doi.org/10.1016/j.commatsci.2016.08.041>.
- [25] J.-O. Andersson, T. Helander, L. Höglund, P. Shi, B. Sundman, Thermo-Calc & DICTRA, computational tools for materials science, *Calphad*. 26 (2002) 273–312. [https://doi.org/10.1016/S0364-5916\(02\)00037-8](https://doi.org/10.1016/S0364-5916(02)00037-8).
- [26] Thermo-Calc software TCFE9 Steels/Fe-alloys database (accessed on 26.09.2019), n.d.
- [27] A. Engström, MOB2 mobility database, Thermo-Calc AB, Royal Institute of Technology, Stockholm. (1998).
- [28] J. Schindelin, I. Arganda-Carreras, E. Frise, V. Kaynig, M. Longair, T. Pietzsch, S. Preibisch, C. Rueden, S. Saalfeld, B. Schmid, J.-Y. Tinevez, D.J. White, V. Hartenstein, K. Eliceiri, P. Tomancak, A. Cardona, Fiji: an open-source platform for biological-image analysis, *Nature Methods*. 9 (2012) 676.

Graphical abstract

